Geochemistry Geophysics Geosystems G3
AN ELECTRONIC JOURNAL OF THE EARTH SCIENCES
Published by AGU and the Geochemical Society

Article
Volume 5, Number 12
30 December 2004
Q12012, doi:10.1029/2004GC000793
ISSN: 1525-2027

Development of oceanic detachment and asymmetric spreading at the Australian-Antarctic Discordance

Kyoko Okino
Ocean Research Institute, University of Tokyo, 1-15-1 Minamidai, Nakano, Tokyo 164-8639, Japan (okino@ori.u-tokyo.ac.jp)

Kohei Matsuda
Ocean Research Institute, University of Tokyo, 1-15-1 Minamidai, Nakano, Tokyo 164-8639, Japan

Now at Japan Meteorological Agency, 1-3-4 Otemachi, Chiyoda, Tokyo 100-8122, Japan (kohei.matsuda@met.kishou.go.jp)

David M. Christie
College of Oceanic and Atmospheric Sciences, Oregon State University, 104 Ocean Administration Building, Corvallis, Oregon 97331-5503, USA (dchristie@coas.oregonstate.edu)

Yoshifumi Nogi
National Institute of Polar Research, 1-9-10 Kaga, Itabashi, Tokyo 173-8515, Japan (nogi@nipr.ac.jp)

Kin-ichiro Koizumi
Ocean Research Institute, University of Tokyo, 1-15-1 Minamidai, Nakano, Tokyo 164-8639, Japan (koizumi@ori.u-tokyo.ac.jp)

[1] The largest known oceanic detachment terrains occur in Segment B3 of the Australian-Antarctic Discordance (AAD). Using newly collected bathymetry, magnetic, and gravity data, we show that Segment B3 is divided into two contrasting second-order segments. The western subsegment, B3W, is characterized by well-ordered, ridge parallel abyssal hills and low mantle Bouguer gravity anomalies. The eastern subsegment, B3E, displays rough, chaotic morphology and includes several megamullions characterized by high mantle Bouguer gravity anomaly values. The crust is estimated to be thinner by a maximum of 3 km in southern B3E. The combination of chaotic morphology with thinner crust supports the idea that the megamullions are exposed footwalls of oceanic detachments. Megamullion terrains are characterized by higher magnetization than adjacent terrains, most likely as a result of serpentinization of peridotite exposed at the detachment surfaces. Detachment surfaces constitute up to 70% of the total area of both ridge flanks younger than 2 Ma in B3E, indicating that oceanic detachments have played a major role in its development. Spreading in B3E has been extremely asymmetric, with higher apparent rates associated with the large detachment surfaces, where up to 75% of the total extension occurred. Similar asymmetric spreading on oceanic detachments is also recognized in Segment B4, suggesting that this is the dominant mode of extension associated with cold mantle and low magma supply in this deepest part of the AAD, where it is confined to a mere 100-km-long section of the AAD spreading axis.

Components: 11,394 words, 11 figures, 1 table.

Keywords: detachment; gravity anomaly; magnetic anomaly model; megamullion; mid-ocean ridge; morphology.

Index Terms: 3035 Marine Geology and Geophysics: Midocean ridge processes; 3045 Marine Geology and Geophysics: Seafloor morphology and bottom photography; 3005 Marine Geology and Geophysics: Geomagnetism (1550).

Received 5 July 2004; **Revised** 17 October 2004; **Accepted** 11 November 2004; **Published** 30 December 2004.

Okino, K., K. Matsuda, D. M. Christie, Y. Nogi, and K. Koizumi (2004), Development of oceanic detachment and asymmetric spreading at the Australian-Antarctic Discordance, *Geochem. Geophys. Geosyst.*, *5*, Q12012, doi:10.1029/2004GC000793.

1. Introduction

[2] The Australian-Antarctic Discordance (AAD) is a unique portion of the world mid-ocean ridge system. The AAD is characterized by its anomalously deep seafloor compared with the standard age-depth curve [*Hayes*, 1988; *Marks et al.*, 1990] and by its rugged, chaotic seafloor morphology [*Christie et al.*, 1998]. Within the AAD, a major isotope boundary within the upper mantle [*Klein et al.*, 1988; *Lanyon et al.*, 1995; *Pyle et al.*, 1992; *Christie et al.*, 2004] divides the Indian MORB province to the west, from the Pacific MORB province to the east. Within the AAD, the ridge axis resembles a typical slow-spreading feature with an axial rift valley [*Palmer et al.*, 1993], though the full spreading rate is high intermediate (72mm/yr, [*Demets et al.*, 1994]). Elevated abundances of highly incompatible elements in basalt lavas indicate that low solidus pressures and low extents of melting characterize the mantle beneath the AAD [*Klein et al.*, 1991], resulting in a thinner crust, as interpreted from with observed positive residual mantle Bouguer anomalies [*Cochran et al.*, 1997; *West et al.*, 1994] and seismic observations of anomalously thin crust [*Kojima et al.*, 2003; *Tolstoy et al.*, 1995]. Off-axis, the depth anomaly forms a large, west-pointing, arcuate shape, indicating that the anomalous lithosphere formation has existed for at least 25 m.y. and has migrated westward at a rate of ~15 mm/yr relative to the spreading center [*Cochran and Talwani*, 1977; *Marks et al.*, 1991]. All these observations support the presence of a cooler, more viscous mantle beneath the AAD [*Kuo et al.*, 1995; *Marks et al.*, 1990, 1991; *West et al.*, 1997]; however, the origin of this thermal anomaly is still controversial. Hypotheses that incorporate direct effects from the mantle flow pattern include: convective downwelling [*Hayes*, 1988; *Klein et al.*, 1988; *Kuo et al.*, 1995; *Veevers*, 1982; *Weissel and Hayes*, 1974]; reduced upwelling [*Kuo*, 1993; *Kuo et al.*, 1996]; cold spot [*Hayes*, 1976]; and passive along-axis flow [*West et al.*, 1997]. *Gurnis et al.* [1998] attributed the origin of the cold mantle to a stagnant slab that subducted beneath the Gondwanaland-Pacific margin during the Cretaceous era.

[3] The anomalous features observed in the AAD are closely related to the underlying mantle structure and dynamics. The thermal anomaly may restrain the melt production beneath the AAD and cause the thin oceanic crust. Spreading rate is in general an important parameter controlling ridge characteristics, but, despite its relatively high spreading rate, the AAD shows magma-starved features that are more usually observed in areas of slow or ultraslow spreading. Therefore another key parameter, the balance between the melt supply affected by thermal anomalies and the plate motion, may play an important role in this anomalous region. The rugged morphology in the area may be due to magma-starved extension [*Christie et al.*, 1998]; however, the detailed tectonics of the axial zone has not been clarified. Recent studies show that an important mode of seafloor spreading at slow and ultraslow spreading ridges is asymmetric extension along long-lived, possibly low-angle, normal detachment faults [*Lagabrielle et al.*, 1998]. These oceanic detachments generally appear as domed highs, with flow line parallel corrugations (megamullions), on which lower crust and/or upper mantle materials are exposed. Oceanic detachment faults are analogous to those that expose metamorphic core complexes on land [*Davis and Lister*, 1988]. This series of fault-bounded tectonic blocks that evolve during long-lived detachment faulting at mid-ocean ridges have been called oceanic core complexes. In this paper, we use the descriptive term "megamullion terrain" to indicate a domed high with a corrugated surface. More than 20 such features have been reported along the Mid-Atlantic Ridge [*Cann et al.*, 1997; *Fujiwara et al.*, 2003; *MacLeod et al.*, 2002; *Tucholke et al.*, 1998] and the Southwest Indian Ridge [*Searle et al.*, 2003]. Proposed regions of origin for sole-out or rooting of oceanic detachment faults include the brittle-plastic transition [*Tucholke et al.*, 1998], melt-rich zones within the lithosphere [*Dick et al.*, 2000], and shallow serpentinization fronts [*Escartín et al.*, 2003]. Exposures on detachment fault surfaces may provide important information on the composition and structure of the lithosphere, and more certainly on tectonic and magmatic processes in magma-starved environments. The AAD is unique in the areal extent and longevity of megamullion terrains, so it is one of the

best places to study oceanic detachments. Moreover, the relatively high spreading rate in the AAD allows us to study the spreading rate dependence of the phenomenon and provides higher spatial/temporal resolution, potentially allowing for more detailed knowledge of the formation and evolution of the oceanic detachments.

[4] In this paper, we present new morphology, magnetic and gravity data, mainly from Segment B3 of the AAD. Using magnetic and gravity data, we examine the variability of spreading rate and crustal thickness, respectively, during the last 2 m.y. We show that the magma-starved spreading is restricted to the relatively short (~100-km) section of the AAD that includes Subsegment B3E and Segment B4. Within this section, spreading is extremely asymmetric and oceanic detachments play a key role in the formation of the anomalous lithosphere.

2. Regional Background

[5] The AAD is a part of the Southeast Indian Ridge (SEIR), which has separated Antarctica from Australia since the Late Cretaceous (Figure 1a). The oldest magnetic lineation between Antarctica and Australia is identified as chron 34 [*Mutter et al.*, 1985], and the breakup between two continents began between 110 and 90 Ma [*Cande and Mutter*, 1982]. The anomalous, rough seafloor of the AAD has been recognizable since chron 21/24 period (~50 Ma). The current spreading rate and direction at 125°E are estimated to be 71.6 mm/yr and 11.1°, respectively, on the basis of the global plate motion model NUVEL-1A [*Demets et al.*, 1994]. The current absolute motion of the Australian Plate in the hot spot reference frame is about 83 mm/yr in direction 11°, in contrast to the almost stationary Antarctic Plate, so the Southeast Indian Ridge is migrating northward from Antarctica at about 35 mm/yr [*Gripp and Gordon*, 1990].

[6] *Weissel and Hayes* [1971] first divided the SEIR south of Australia into three zones, Zone A, B, and C from east to west (Figure 1a). Zone A and Zone C west of ~116°W show "fast spreading" features, with no axial rift valley and relatively smooth off-axis morphology. Zone B, from 120°E to 128°E, is characterized by deep seafloor, high off-axis bathymetric relief and prominent axial valleys, and has therefore been called the Australian-Antarctic Discordance (AAD) [*Hayes and Conolly*, 1972]. Five segments are recognized within Zone B, from the westernmost B1 to the easternmost B5 [*Vogt et al.*, 1983]. The axial zone between B3 and B5 was mapped by *Palmer et al.* [1993]. Segments B3 and B4 are offset by the Lutana nontransform discontinuity, while the other segment boundaries are sharp transform faults. Prior to this study, off-axis areas have been mapped only in Segments B4 and B5 [*Christie et al.*, 1998]. The B4 off-axis area is extremely anomalous, showing chaotic bathymetry including two megamullion terrains. In Segment B5 a west pointing V-shaped boundary marks the transition between the chaotic AAD and the well-ordered abyssal hill terrain of Zone A. There have been no off-axis surveys in the western AAD, so the western limits of the chaotic terrain and of anomalous crustal accretion were not known prior to this study.

[7] A number of previous studies contribute to the conclusion that anomalously cool upper mantle and thin crust exist beneath the AAD. Geodynamic studies by [*Kuo et al.*, 1995; *Marks et al.*, 1991; *Marks and Stock*, 1994; *West et al.*, 1994] have indicated that the mantle beneath the AAD is about 150°C colder than average using gravity/topography ratios. Numerical modeling [*West et al.*, 1994] shows that a small decrease in upper mantle temperature will produce a significantly (at least 3 km) thinner crust. Refraction seismic studies in the AAD have also indicated an anomalous crustal structure. *Tolstoy et al.* [1995] showed that, within Segment B5, the crust is quite thin (4.2 km), with a relatively thick layer 2 (~3 km) and an unusually thin layer 3 (~1.2 km). A more recent refraction experiment [*Kojima et al.*, 2003] showed an anomalous velocity model in Segment B4, where the P wave velocity gradually increases with depth, reaching 7.8 km/s at only 3.6 km.

3. Data Acquisition and Processing

[8] Swath bathymetry, gravity and magnetic data for Segment B3 of the AAD were acquired in 2002 on board the R/V *Hakuho-Maru* (KH01-3, Leg. 3). The track lines were laid out NNE-SSW along flow lines, extending to 75 km off-axis on both ridge flanks (Figure 1b). Track spacing was 5 nautical miles, yielding almost complete bathymetric coverage. The survey area covers the whole of B3, from the Warringa transform fault at 124°E to the Lutana nontransform discontinuity (NTD) at 125°05′E.

3.1. Bathymetry

[9] Swath bathymetry data were collected by the SeaBeam 2120 system, which comprises 110 beams

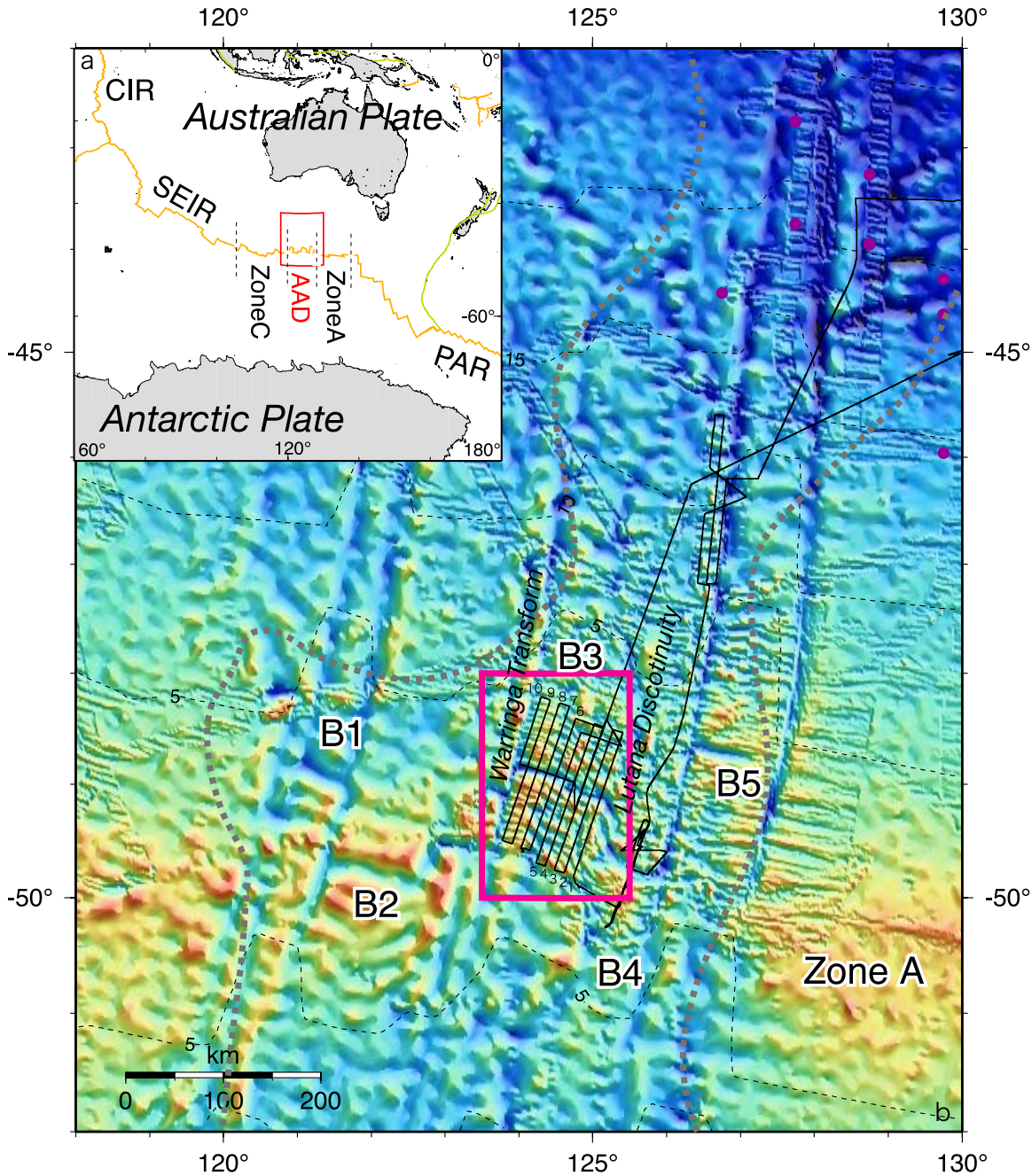

Figure 1. (a) (inset) The plate tectonic setting and the location of the AAD. Yellow and green lines indicate divergent and transform-fault boundaries, respectively. CIR, Central Indian Ridge; SEIR, Southeast Indian Ridge; PAR, Pacific-Antarctic Ridge. (b) Bathymetry around the AAD. Our newly obtained data (B3) are combined with previous multibeam survey data [*Christie et al.*, 1998; L. Géli, personal communication, 2000] and ETOPO2 (National Geophysical Data Center, 2001). The AAD (Zone B) is divided into five segments, B1 to B5. Thin black lines with line numbers indicate the KH01-3 track lines used in this study. Solid circles show ODP Leg 187 drill sites. Thin black dashed lines with numbers are isochrons by *Müller et al.* [1998]. Thick gray dotted line is the 400-m depth anomaly contour by *Marks and Stock* [1994]. Pink box marks the area shown in Figures 2, 3, 6a–6f, and 9.

at the surveyed depths operating at 20 kHz. The horizontal resolution ranges from 70 to 120 m, and the average swath width is 11 km. The sound velocity correction used real-time data from the surface water velocity meter and the results of CTD and XBT observations in the area. We removed extreme depth variations from the outer edge of the swath using MB system [*Caress and Chayes*, 1996]. The chosen grid size is 100 m and the grid data set is masked to approximately the original swath coverage allowing interpolation of small gaps within 1 km. A complete bathymetry grid without gaps was also created to do the Fourier transform analysis described below, by merging the compiled bathymetry of previous surveys [*Christie et al.*, 1998; L. Géli, personal communication, 2000] and ETOPO2 (National Geophysical Data Center, 2001). No adjustment among three data sets was done during compilation, for the average difference between newly collected data and data from previous surveys is less than 10 m. Depths from ETOPO2 shows larger disagreement with ship-derived data (>60 m), then the areas without ship bathymetries were masked in results.

3.2. Gravity

[10] Gravity data were acquired using the NIPRORI type shipboard gravity meter. Drift and Eötvös corrections were made and the free-air gravity anomaly was calculated subtracting the standard gravity using Gravity Formula 1980. The maximum and root-mean square crossover errors were 8.1 mGal and 3.5 mGal, respectively. Satellite gravity data [*Sandwell and Smith*, 1997] were merged to fill the data gap, and a 1 km spacing grid was created.

[11] In order to estimate the crustal thickness and/or subsurface density variations we calculated mantle Bouguer anomalies (MBA) by subtracting from free-air gravity anomaly the predicted gravity effects of seafloor relief and a 4 km thick model crust [*Kuo and Forsyth*, 1988; *Lin and Phipps Morgan*, 1992; *Parker*, 1972; *Prince and Forsyth*, 1988]. Assumed water/crust and crust/mantle density contrasts are 1770 kg/m^3 and 600 kg/m^3, respectively. The effect of sediment was neglected, for the sediment thickness is negligible at the active spreading axis. We further calculated residual mantle Bouguer anomalies (RMBA) to remove the effects of lithospheric cooling. The thermal model was calculated using the three-dimensional passive upwelling model of [*Phipps Morgan and Forsyth*, 1988], where the transform effect was incorporated. The resulting temperature field was converted into density variation [*Prince and Forsyth*, 1988], and then the gravity anomaly caused by density variation on each model subsurface layer was calculated by upward continuation. We also estimated a model of crustal thickness variation by downward continuation of RMBA to an assumed mean depth of 8 km (4 km of average water depth plus 4 km crust) [*Kuo and Forsyth*, 1988]. A cosine tapered low-pass filter between 25 km and 35 km was applied to reduce the noise. The MBA, RMBA and crust thickness variation assuming a 6 km thick crust were also calculated for discussion.

3.3. Magnetism

[12] The magnetic data were acquired every 30 seconds using a surface-towed proton precession magnetometer. The data were corrected for the International Geomagnetic Reference Field [*Mandea et al.*, 2000] to obtain magnetic anomalies. On three of the five survey days, the magnetic data suffered from geomagnetic disturbances when Kp (mean value of the geomagnetic field disturbance levels in the two horizontal field components observed at selected stations) sum index values were 28−, 28+, 23+, respectively. Crossover errors (total 17 points) were rather large, presumably due to the disturbance; the maximum crossover error was 125 nT and the root-mean square error was 52 nT. The closest available magnetic observatory is at Macquarie Island (54.5°S, 158.95°E) 2500 km east of the study area, so an appropriate diurnal correction could not be obtained by directly using the data from the station. We shifted the Macquarie station magnetic data, taking the time lag at the AAD into account, and then calculated our geomagnetic variation model using a stochastic inversion to minimize crossover errors. This correction reduced the maximum and root-mean square cross over errors to 25 nT and 10 nT, respectively. No previous off-axis ship-derived magnetic data were known in segment B3, and the aeromagnetic data in this area [*Vogt et al.*, 1983] show good correlation with the corrected magnetic anomaly pattern.

[13] We compared the corrected magnetic anomalies with synthetic anomaly profiles and identified a sequence of magnetic anomalies on the basis of the *Cande and Kent* [1995] timescale. The identified anomaly chrons and their ages are listed in Table 1. We linked the anomaly picks on each profile to draw the isochrons, and interpolated along flow lines to create a seafloor age grid from which spreading rates were calculated. The degree

Table 1. Identified Geomagnetic Anomalies

Polarity Chron	Age, Ma
c1o (Brunhes/Matuyama boundary)	0.780
c1a (Jaramillo subchron)	1.030
c2 (Olduvai subchron)	1.860
c2ay (Matuyama/Gauss boundary)	2.581
c2a-1 (Kaena subchron)	3.075
c2a-2 (Mammoth subchron)	3.275
c2ao (Gauss/Gilbert boundary)	3.580
c3-1 (Cochiti subchron)	4.235

of spreading asymmetry is calculated for each flank as the ratio (expressed as percentage) of the area accreted on that flank to the total accreted area for a given age interval. Thus conjugate values from opposite flanks should sum to 100%. An asymmetry ratio of 50% equates to symmetrical spreading, while conjugate values of 0 and 100% equate to complete asymmetry.

[14] We calculated crustal magnetization to remove skewness and to correct for effects of bathymetry using the three-dimensional inversion method of [*Parker and Huestis*, 1974] and [*Macdonald et al.*, 1980]. The direction of seafloor magnetization was taken to be the same as the geocentric axial dipole field, and a 500 m magnetized layer thickness was assumed. The upper surface of the magnetized layer was assumed to be the same as the seafloor, for the sediment thickness of the area is very thin. A Taylor expansion up to the fifth order was carried out, and ten iterations brought sufficient convergence of the solution. A band-pass filter, cosine tapered at short wavelength between 8 to 10 km and at long wavelength between 260 and 300 km, was applied to each iteration to stabilize the solution. Sufficient annihilator was added so as to give about equal amounts of positive and negative magnetization amplitude and to give appropriate positions of geomagnetic reversals. The aeromagnetic data [*Vogt et al.*, 1983] were downward continued and merged with our onboard data set in the marginal areas to create a grid data without gaps for Fourier transformation.

4. Results

4.1. Morphology

[15] The shaded relief map is illuminated from the north with a 100 m contour interval (Figure 2) and the tectonic fabric extracted from the swath bathymetry is shown in Figure 3. The ridge axis is characterized by a 5- to 15-km-wide, 1500- to 2000-m-deep axial rift valley, which is anomalous for the high intermediate spreading rate. A right-stepping, 8-km nontransform offset at 124°35′E separates second order segment B3W from B3E. The B3W and B3E axes overlap by 15 km and the eastern end of the B3W axis is accompanied by eastward-pointing, V-shaped pseudofaults indicating rift propagation. Minor ridge structures ~100 m high within the rift valley, that are interpreted as neovolcanic zones, are developed in B3W and in the western half of B3E (Figure 4). The off-axis trace of the nontransform discontinuity (NTD) between B3W and B3E extends across the entire survey area as a highly sinuous, deep region. The sinuous nature of this trace indicates repeated, ''dueling'' decline and growth of the two subsegment axes. The maximum variation in subsegment length is about 40 km, and the average periodicity of the fluctuation is about 0.4 m.y.

[16] The morphology of the off-axis area of B3W contrasts in a striking way with that of B3E. The B3W off-axis area consists of well-ordered, rift-parallel abyssal hills. The average water depth of the southern flank is shallower (~3400 m) than that of the northern flank (~3700 m). The wavelength and relief of the abyssal hills increase as they step away from the current rift axis, which most likely reflects the continued growth of normal faults [*Macdonald et al.*, 1996]. In contrast to the normal abyssal hills of B3W, the off-axis morphology of B3E is highly anomalous. Seafloor relief is high and variable and there is no clear correlation between depth and distance from the axis within the survey area. The seafloor fabric is a chaotic mixture of domes, with rift-parallel and rift-oblique abyssal hills and several megamullions (Figure 5). Most previously reported megamullions are located at inside corners of slow-spreading axial-valley-transform intersections. In contrast, megamullions within the AAD, including those of B3E shown here, and those of Segment B4 [*Christie et al.*, 1998] are distributed across the entire (sub)segment. Although the B3E megamullions are developed both on southern and northern flanks, the southern megamullions are larger and the corrugations are more continuous.

[17] The largest B3E megamullion, at the eastern inside corner, has continuous corrugations 50 ~ 55 km long. It consists of two flow line parallel bathymetric highs with prominent, smaller-scale corrugations on their surfaces (Figure 5a). This is

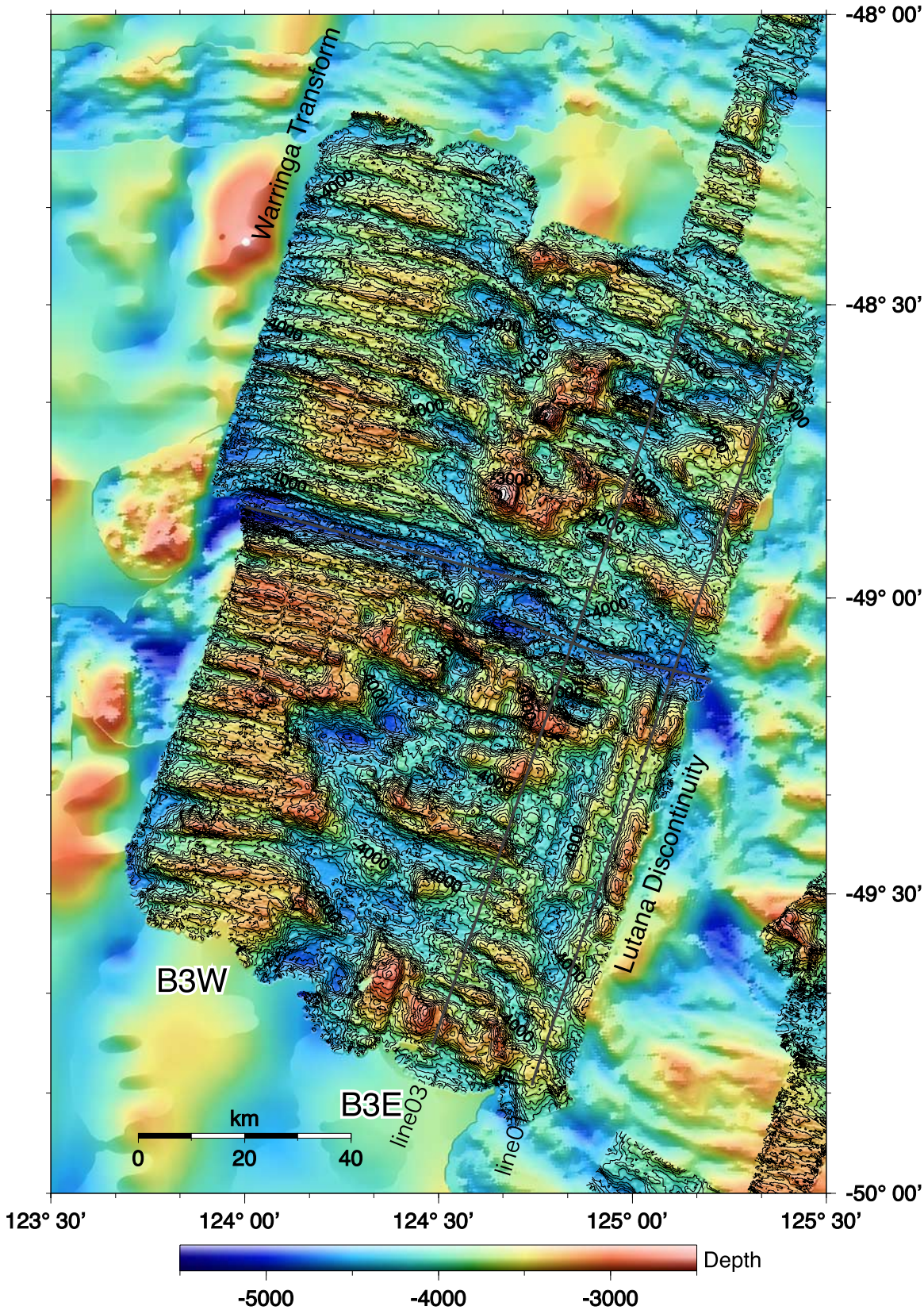

Figure 2. Shaded relief with bathymetry contours in segment B3. Contour lines are drawn only for the area of the newly obtained data set. Contour interval is 100 m. Subsegments B3W and B3E show strong contrast in morphology. Gray lines indicate the locations of across- and along-axis profiles shown in Figure 7.

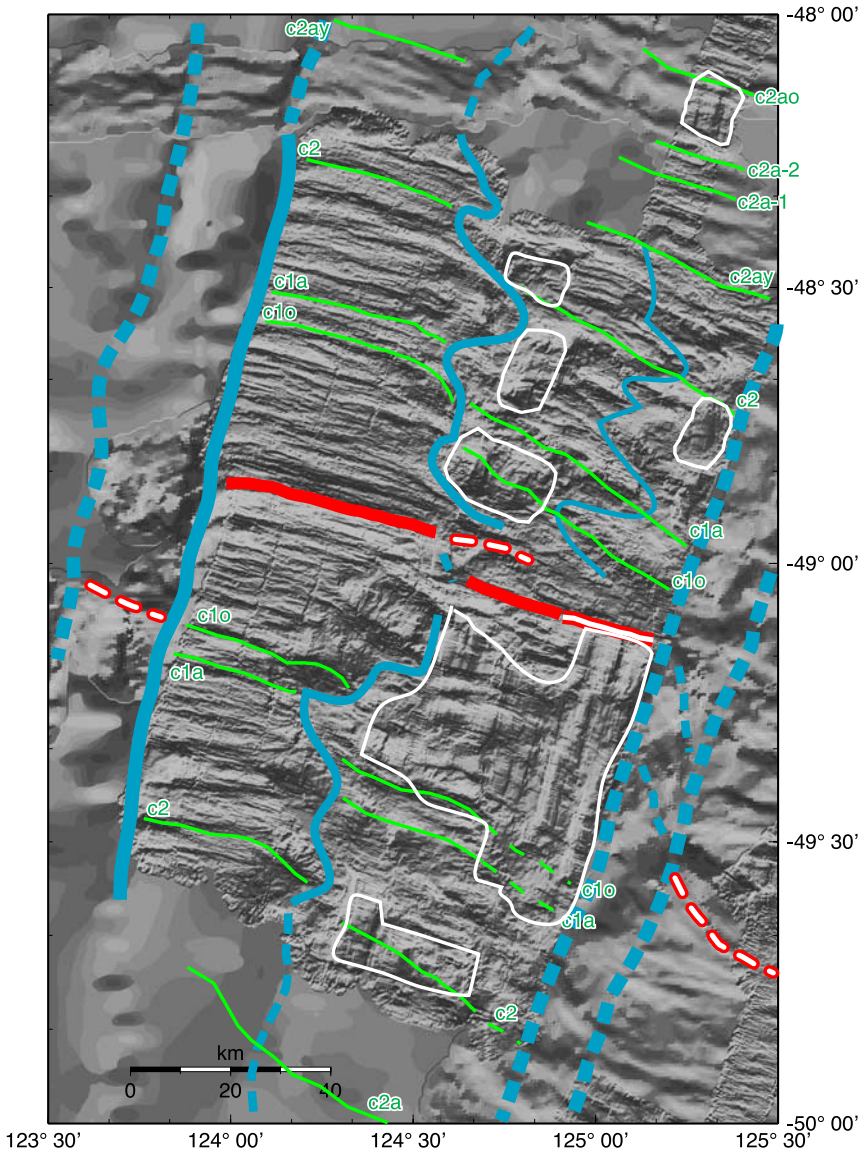

Figure 3. Geological interpretation and identification of magnetic anomalies superimposed on shaded bathymetry. Bathymetry is illuminated from directions 015° and 285°. Thick red lines are rift axes with neovolcanic zones; red-white lines are rift axes without neovolcanic zones. Blue lines indicate transforms/fracture zones or nontransform discontinuities (NTDs). Areas with well-developed, flow line parallel corrugations are surrounded by white lines. Green lines with labels show the identified magnetic anomalies (see Figure 9).

the largest known megamullion in the AAD, and is larger than any known Mid-Atlantic Ridge megamullion [*Tucholke et al.*, 1998]. The termination of this megamullion (for terminology, see *Tucholke et al.* [1998]) at its northern end coincides with the axial rift valley (Figure 4), suggesting that the detachment fault is still active. Farther from the inside corner, an adjacent group of smaller mullion structures is located next to the largest megamullion terrain. This group consists of several small corrugated domes, each about 10 km wide (E-W) and 5–10 km long (N-S), that are cut by three or four rift parallel escarpments (Figure 5b). To the south of this area, a 1000 m high, rift-parallel ridge marks the breakaway for this terrain. To the north, the corrugations terminate at a distinct E-W lineament marking the termination of the detachment fault. Three or four normal abyssal hills separate the termination from the neovolcanic zone in this western part of B3E. The boundary between these two megamullion terrains on the southern flank appears to coincide with a minor, third order segment boundary. On the north flank, this boundary can also be traced as a sinuous deep. South of

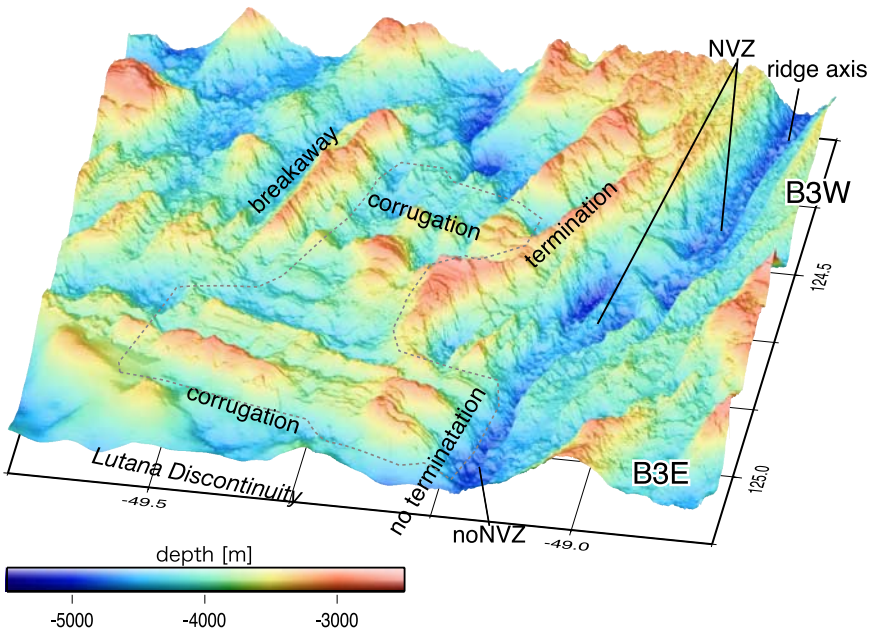

Figure 4. Three-dimensional view of the southern flank of B3E from 085° direction. Area surrounded by gray dotted line is the megamullion terrain in southern B3E. Minor ridge structure within the rift valley is interpreted as a neovolcanic zone, which is indicated as NVZ in the figure. Vertical exaggeration is ~2.0.

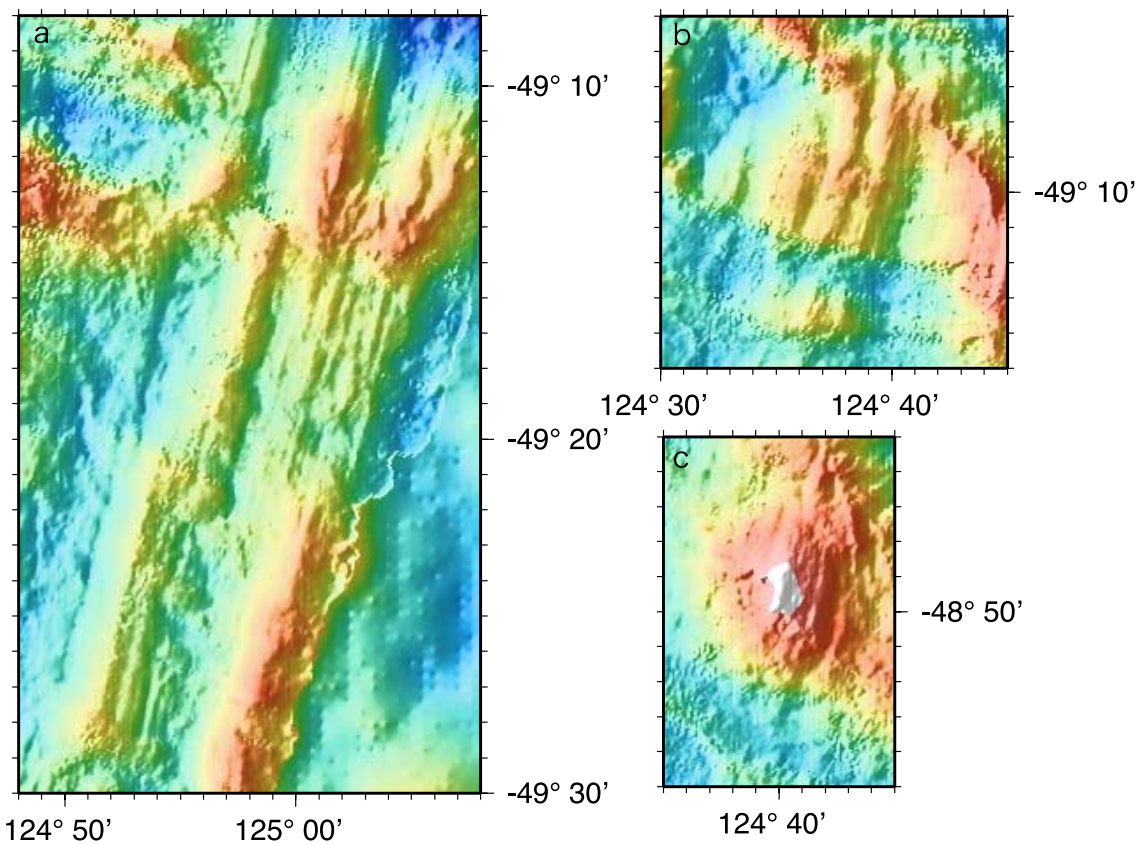

Figure 5. Close-up view of megamullions (a and b) on southern flank of B3E and (c) on northern flank of B3E. Color scale is as same as that used in Figure 2. Bathymetry is illuminated from direction 285°.

49°40′S, a megamullion terrain consisting of four 10 km wide, 500 m high domes extends E-W across B3E and south beyond the survey area.

[18] The megamullion terrains on the southern flank of B3E are all characterized by closely spaced corrugations of 100- to 200-m wavelength, 50-m relief, and 5- to 10-km minimum length. Megamullion terrains also occur on the northern flank of B3E, but they are relatively small and widely separated. Each consists of a single dome, 10–20 km across and 1000–1500 m high (Figure 5c). They are sparsely corrugated, randomly distributed and separated by rift-parallel abyssal hills. Breakaway and termination traces are ambiguous. In all these characteristics, they more closely resemble megamullion terrains along the slow-spreading Mid-Atlantic Ridge.

4.2. Gravity Anomalies

[19] The free-air, mantle Bouguer and residual mantle Bouguer gravity anomalies are shown with estimated variations of crustal thickness in Figures 6a–6f. The free air anomaly pattern (Figure 6a) correlates well with bathymetry. The mantle Bouguer anomalies (MBA) are about 10 mGal higher in B3E than in B3W (Figure 6b). In both subsegments the MBA decreases from the segment ends to the center. In B3E a weak negative trough is confined to the western (magmatic) part of the rift valley. The along-axis variations in MBA values within subsegments B3W and B3E are 17 mGal and 13 mGal, respectively (Figure 7a). MBA values gradually increase away from the axis, mainly due to the effect of plate cooling.

[20] The residual mantle Bouguer anomaly (RMBA) is calculated to remove the effect of plate cooling (Figure 6c). Our calculated RMBA values decrease away from the axis; this tendency is likely due to an overestimate of plate cooling rates and/or our disregard of buoyancy effects. The RMBA is markedly higher in B3E, where the high RMBA (∼30 mGal) area is located south of the axis, near the termination of the western B3E megamullion terrain. The MBA values in the megamullion on the southern flank of B3E are approximately same as those at same distance from the axis in the northern flank, therefore the high RMBA is consistent with asymmetry of plate cooling, which may indicate asymmetry of spreading rate described in next section. However, the megamullion terrains have generally higher Bouguer anomalies, with RMBA values 5∼10 mGal higher than in surrounding areas. The high gravity anomalies associated with megamullions are also clearly shown in across-axis profiles (Figures 7b and 7c).

[21] Assuming that variations in RMBA are caused only by differences in crustal thickness, we estimated variations of crustal thickness (Figure 6d). The crust of B3W is, on average, thicker than that of B3E. In northern B3W, the crust is estimated to be thicker by a maximum of 3 km. The megamullion terrains of southern B3E and those of northern B3E near the NTD have thinner crust. Thinner crust is also observed along the Lutana NTD and close to the axis at the 124°40′ (B3W/B3E) NTD. The Warringa Transform Fault does appear to have thinner crust, but this may be due to the poor data coverage. Estimates of crustal thickness involve significant uncertainty, because gravity anomalies can also be caused by upper mantle temperature and density variations, density decreases associated with serpentinization or other alteration and other factors. The 3 km of crustal variation was obtained as a result of downward continuation of RMBA using 600 kg/m^3 density contrast across the Moho, so the gravity anomaly can also be explained by different layer thickness and density contrast models, for example assuming serpentinized mantle material for subsurface layer.

[22] The MBA, RMBA and crustal thickness variation assuming a 6 km thick crust were also calculated (Figure 6e and 6f). The difference of a reference depth does not change any of the basic results of the analysis. The amplitude of the crustal thickness variation is larger in a 6km thick crust model, though the general pattern is as same as in a 4 km thick crust model. We do not have any seismic profiles in segment B3 to examine the Moho depth derived from gravity analysis; however, a 4-km-thick crust model is preferable because the previous refraction results in B4 [*Kojima et al.*, 2003] and B5 [*Tolstoy et al.*, 1995] shows 3.6 ∼ 4.2 km crust thickness.

4.3. Magnetic Anomalies

[23] We used magnetic isochrons identified from the magnetic anomaly map to calculate the detailed history of plate motion and variations in spreading rate. Model profiles allowing asymmetric spreading are shown for comparison with observed profiles (Figure 8). Good fits were achieved with little asymmetry for profiles in B3W (lines 07-10), with poorer fits for the southern parts of lines 01 and 02 in B3E. Anomalies are more strongly positive values and less variable over megamullions. The better fits along lines 01-02 were achieved by

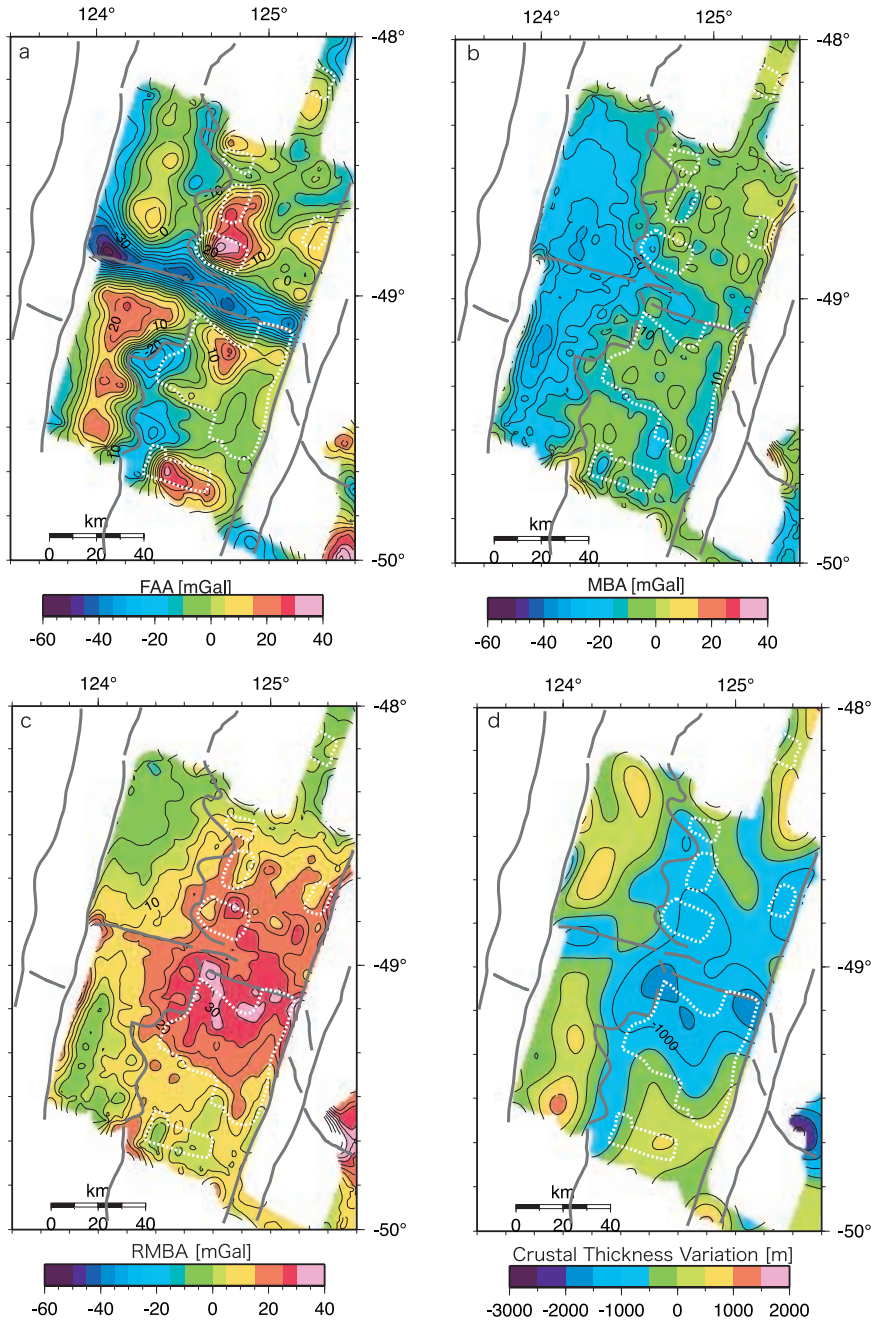

Figure 6. (a) Free-air gravity anomaly map. Contour interval is 5 mGal. Gray lines show rift axes and transform fault/NTDs. White dotted circles outline megamullion terrains. (b) Mantle Bouguer gravity anomaly (MBA) contoured at 5 mGal. (c) Residual mantle Bouguer gravity anomaly (RMBA) calculated from MBA and theoretical lithosphere cooling effects. Contour interval is 5 mGal. (d) Relative crustal thickness variations calculated by downward continuation of RMBA. Contour interval is 500 m. A 4-km-thick crust is assumed for MBA calculation. For Figures 6e and 6f, a 6-km-thick crust is assumed for MBA calculation: (e) Mantle Bouguer gravity anomaly (MBA) contoured at 5 mGal. (f) Relative crustal thickness variations calculated by downward continuation of RMBA.

introducing induced magnetization; however, this will be discussed in a later paper. Because the line 06 repeatedly crosses the highly sinuous NTD trace, there are large discrepancies between model and observed profiles. Anomalies up to c2 (Olduvai subchron) were identified on both northern and southern flanks of B3W and B3E. Older anomalies from c2ao to c2 were also identified on the northern flank of B3E using a transit line. Anomalies c1o (B/M boundary) and c1a (Jaramillo subchron) were

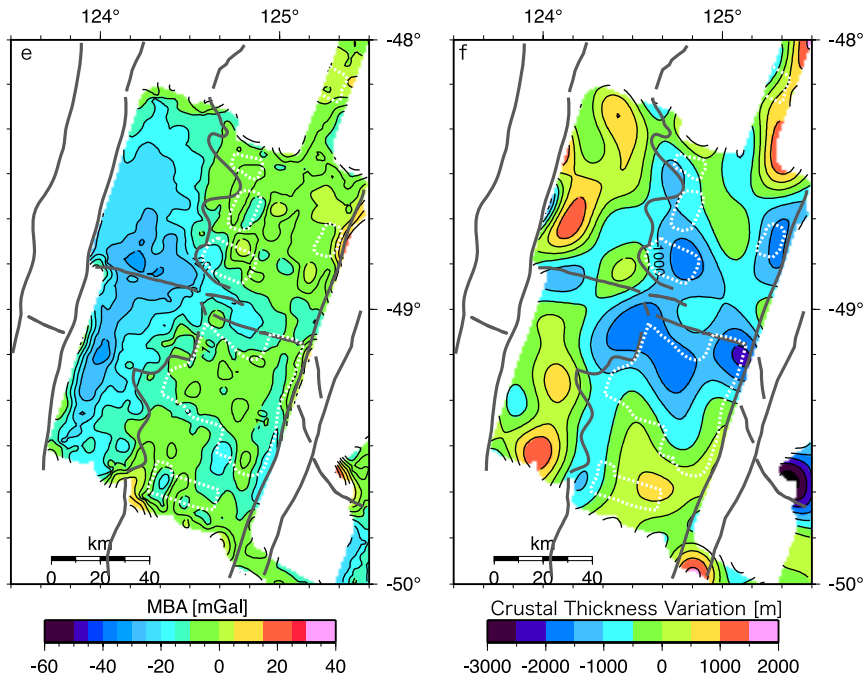

Figure 6. (continued)

identified on most of track lines (Figures 8 and 9a). The average half spreading rate in segment B3 from 1.8 Ma to present is about 38 mm/yr, consistent with the global plate motion model [*Demets et al.*, 1994]. During this period, however, marked variations in spreading rate can be clearly recognized. Figures 9b and 9c show variations in half-spreading rate and spreading asymmetry, respectively. For southern B3W, the spreading rate is almost constant at 40 mm/yr from c2 to present, while for northern B3W, half-spreading rates increased from 30 mm/yr between c2 and c1o to 38 mm/yr since c1o. Overall, the southern flank has spread faster, but the degree of asymmetry is less than 5% (Figure 9c).

[24] In contrast to the relatively small asymmetry in B3W, the spreading rate in B3E has been highly variable, both through time and from west to east across the subsegment. For southern B3E, the half-spreading rate has varied consistently from west to east as well as with age. Half-spreading rates have increased from 32/35 mm/yr (west/east) between c2 and c1o, to 50/55 mm/yr since c1o. Across northern B3E, there was no west-east variation from c2ao to c2, but the half-spreading rate decreased from 50 to 30 mm/yr. Between c2 and c1a, the half-spreading rate increased from west (27 mm/yr) to east (42 mm/yr), but since that time the half-rate has decreased from west (30 mm/yr) to east (15 mm/yr). Prior to c1o, the degree of spreading asymmetry was small (less than 5%), but it has increased dramatically, exceeding 20% from c1o to present (Figure 9c). During the past one million years, the spreading in B3E has been highly asymmetric, with rates exceeding 50 mm/yr across the megamullion terrains to the south. Throughout this time, however, the full-spreading rate has remained at 79–80 mm/yr, almost the same as in the other parts of the Southeast Indian Ridge. The intense, localized spreading asymmetry over the last 0.5 m.y. is a remarkable contrast to the generally small asymmetry that characterizes Segment B3 through the time encompassed by the survey area. The loci of high asymmetry generally correspond to the major oceanic detachment surfaces, with the faster spreading flank corresponding to the megamullion terrains. More detailed discussion and the asymmetry in the neighboring segments are written in the next section.

[25] The magnetization intensity distribution map (Figure 9d) shows high magnetization areas along the NTDs and in the megamullion terrains of southern B3E. The magnetization at the segment ends is strongly positive relative to the surrounding seafloor regardless of whether polarity is normal or reversed. The high positive magnetization, both at segment ends and across the southern B3E megamullion terrains is most likely caused by induced magnetization associated with peridotite serpentinization [*Pariso et al.*, 1996; *Pockalny et al.*, 1995; *Tivey and Tucholke*, 1998] and the detachment

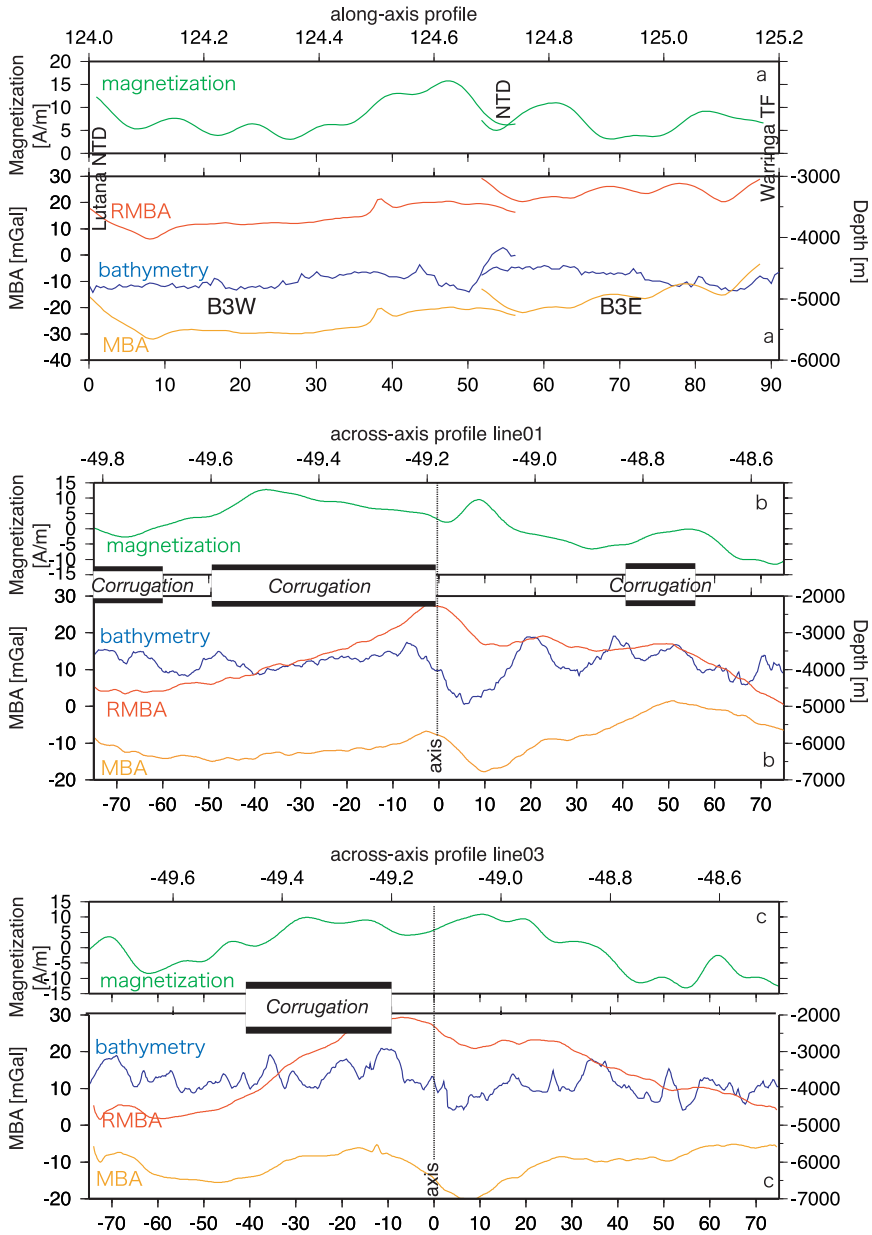

Figure 7. Magnetization, bathymetry, mantle Bouguer anomaly (MBA), and residual mantle Bouguer anomaly (RMBA) profiles from Segment B3. The locations of profiles are shown in Figure 2. (a) Along-axis profile from B3W to B3E. (b and c) Across-axis profiles in B3E, crossing large mullion structures with corrugated surfaces. Horizontal scale is different between (a) along- and (b and c) across-axis profiles.

surface. Our analysis of the magnetization structure of the area using detailed forward modeling will be discussed in a later paper.

5. Discussion

5.1. Detachment Hypothesis

[26] In recent years, asymmetric extension along low-angle normal detachment faults has been increasingly recognized as an important mid-ocean ridge process, especially in magma-poor and slow spreading systems. More than twenty seafloor terrains interpreted as detachment surfaces have been reported from on- and off-axis areas along the Mid-Atlantic Ridge (MAR) [*Blackman et al.*, 1998; *Cann et al.*, 1997; *Fujiwara et al.*, 2003; *Ranero and Reston*, 1999; *Tucholke and Lin*, 1994; *Tucholke et al.*, 1998]. These features are usually characterized by dome-like bathymetric highs, with

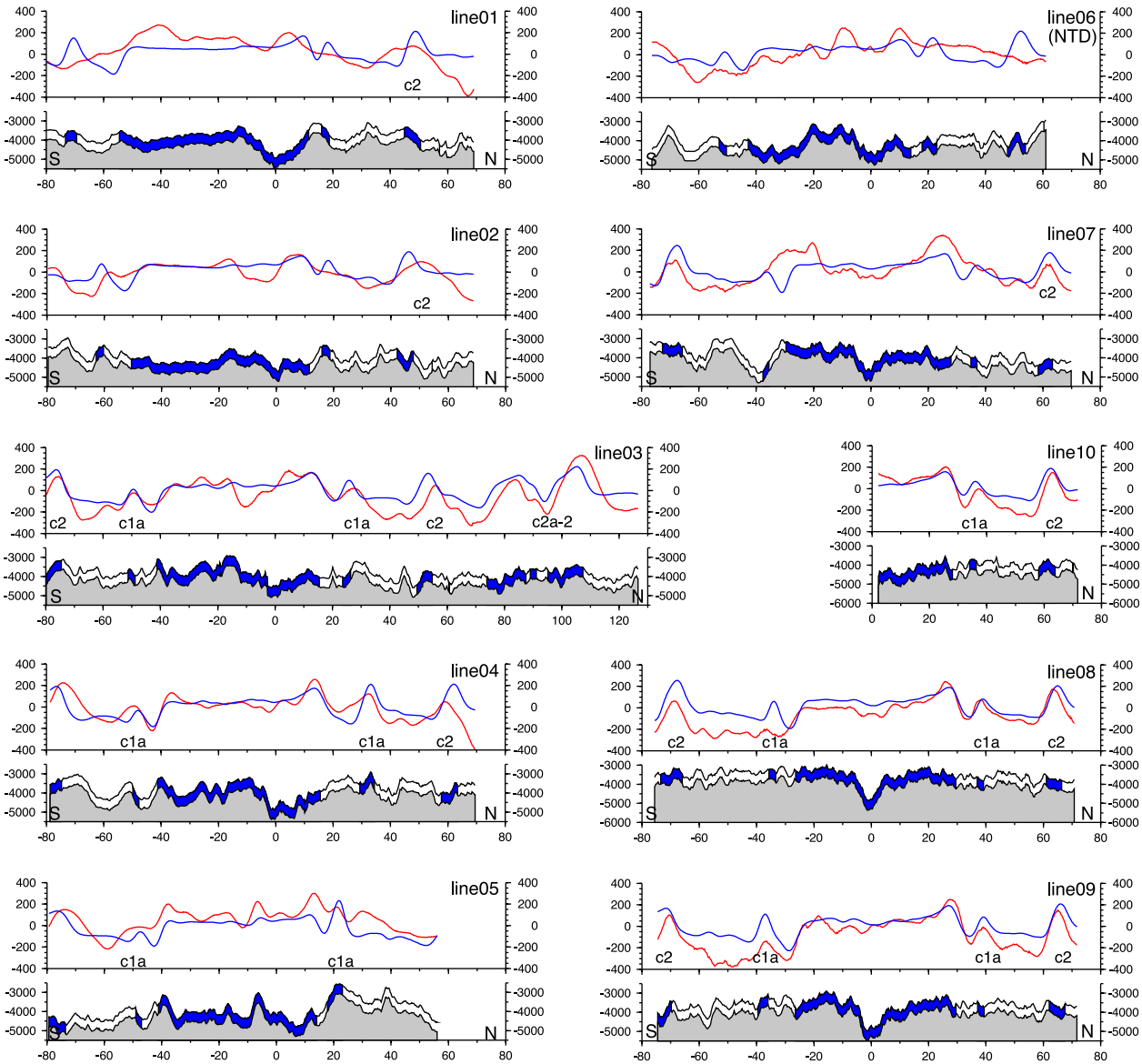

Figure 8. Model profiles (blue) using the geomagnetic reversal timescale of *Cande and Kent* [1995] with observed magnetic anomaly profiles (red) and bathymetry. We assume a constant 500-m-thick magnetic layer draped on the bathymetry with a uniform ±5 A/m magnetization. Locations of lines are shown in Figure 1.

flow line parallel corrugations and striations, and delineated from normal abyssal hill terrains by narrow sublinear valleys that define the "breakaway" and the "termination", the lines at which the exposure of the detachment surface at the seafloor began and ended, respectively. Most of these morphological features, named megamullions, are associated with gravity highs indicating denser subsurface structure. Dredge and drill sampling typically returns deep-seated, gabbro and peridotite samples, in addition to cataclastic (fault-generated) rock types and highly deformed greenschist facies assemblages [*MacLeod et al.*, 2002]. These observations indicate that the corrugated surface is the exposed footwall of an oceanic detachment fault, analogous to core complexes on land [*Davis and Lister*, 1988]. The oceanic detachments along the MAR are mostly located at present or remnant inside corners of ridge-transform intersections, where the melt supply is presumed to be smaller than that at segment centers. Very similar features have been also reported at ultraslow spreading systems [*Searle et al.*, 2003], at some intermediate spreading-rate systems [*Martinez et al.*, 1998; *Mitchell et al.*, 1998; *Ohara et al.*, 2001] and from Segment B4 of the AAD [*Christie et al.*, 1998].

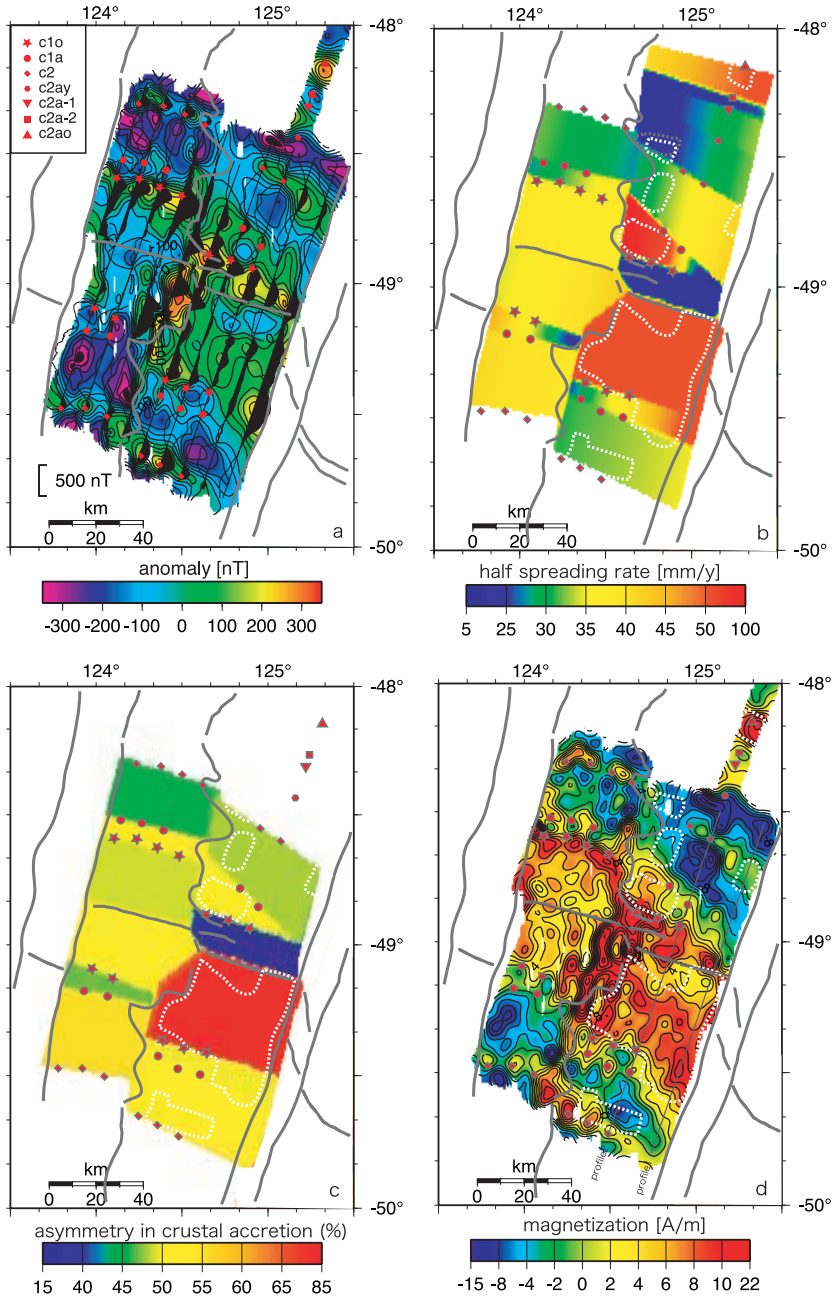

Figure 9. (a) Magnetic anomaly map. Contour interval is 20 nT. The anomaly profiles along track lines are shown in wiggles (positive anomalies are shaded). Red symbols mark anomalies (see Table 1) picked along ship track. Gray lines show rift axes and transform fault/NTDs. (b) Half spreading rates calculated for intervals between anomaly picks. White dotted lines outline megamullion terrains. Large variations in spreading rate are observed in B3E. (c) Crustal accretion rates of conjugate plates, expressed in terms of the "degree of asymmetry" (see text). A "50%" asymmetry equates to symmetrical spreading. (d) Crustal magnetization calculated from magnetic anomaly amplitudes. Contours are at 2 A/m intervals.

[27] The B3E megamullion terrains described here are extremely anomalous in their broad areal extent and in their duration. In B3E, domed features with prominent or subtle corrugations occupy about 70% of the seafloor younger than 2 Ma, indicating that "magma-starved" extension dominates over "magmatic" accretion, and has been the dominant mode of spreading for at least two million years. The largest mullion structure, at the inside corner of the eastern end of Segment B3, is about 50 km long, about twice the average length of megamullions in the MAR. Megamullion structures occur

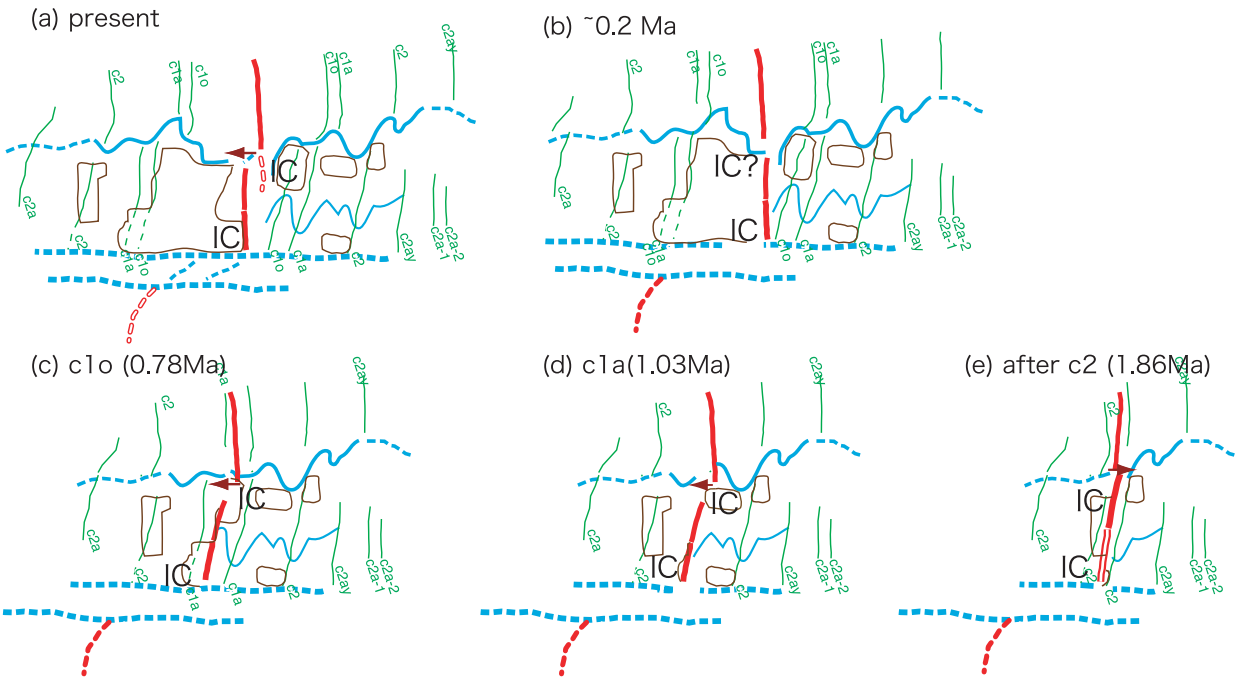

Figure 10. One hypothesis for the evolution of B3E and the origin of small detached terrains in the northern B3E ("reversal of detachment polarity"; see text). IC indicates inside corner. Green lines are isochrons. Red and blue lines are spreading centers and nontransform/transform offsets, respectively. Megamullions are surrounded by brown lines. The offset between B3E and B3W is shown by brown arrows.

across the width of southern B3E, in clear contrast to the well-ordered normal abyssal hills in B3W. A shortage of melt supply extends along the entire B3E axis and is not limited to the segment ends. Small, chaotic domes are also widely distributed on the northern flank of B3E. We propose two alternative hypotheses for the origin of these small detached terrains.

5.1.1. Origin of Detached Terrains by Reversal of Detachment Polarity

[28] The small northern megamullions may have formed when the polarity of detachment was reversed for short periods. Like most megamullion terrains elsewhere, the major B3E megamullion adjoins the Lutana Discontinuity, the eastern boundary of Segment B3, on the southern flank, at the inside corner of a right-stepping offset. A small northern terrain also adjoins the Lutana Discontinuity just after c2 chron. Along the western boundary of B3E, on the other hand, megamullion terrains are distributed on both flanks. The southernmost megamullion terrain began forming prior to the survey coverage and terminated just after c2 chron. A younger southern terrain in western B3E began forming close to c1o and terminated relatively recently. The three small northern megamullions in western B3E formed: before c2, just before c1a, and between c1a and c1o. The offset between B3W and B3E is small and its sinuous off-axis trace indicates that it is unstable, migrating over ~40 km from east to west as a result of small ridge jumps or propagation events. Each of the northern megamullions coincides with a westward excursion of the B3W/B3E boundary trace (Figure 9), suggesting that it occurred at an inside corner during a period when B3E was active and growing. As the migration of the offset reversed, the transformation from inside to outside corner position may have terminated the active detachment and initiated a new fault with reversed polarity. Similar, long-lived magma-starved spreading segments with changing detachment polarity have been reported from off-axis areas of the easternmost Southwest Indian Ridge at 64–65° E [*Cannat et al.*, 2003]. A possible model for segment evolution involving such transient detachment-polarity reversals is illustrated in Figure 10.

5.1.2. Origin of Detached Terrains by Lithosphere Transfer During Detachment Relocation

[29] The small northern B3E megamullions may represent blocks of lithosphere that were trans-

ferred from the southern to the northern plate as the locus of displacement shifted southward to a new fault plane. As described in the preceding section, the northern B3E megamullion terrains more closely resemble their counterparts along the slow-spreading Mid-Atlantic Ridge than those in southern B3E. Further, they coincide in apparent age with the southern flank megamullion terrains, with no complementary gaps on either flank. Their origin does not seem to be attributable to a simple detachment fault model. One possible explanation is that the northern terrains were formed during a transient periods when extension rates were slowing, immediately prior to deactivation of the detachment fault plane. Initiation of a new detachment farther to the south would transfer these localized, ''slow-spread'' terrains from the southern to the northern flank and reinstate the formation of a faster-spreading terrain on the southern flank. The transfer of a megamullion terrain from one flank to the other has also been proposed for the Fifteen-Twenty Fracture Zone area of the MAR [*Fujiwara et al.*, 2003].

[30] Although no direct observation was reported on the crustal structure beneath the B3 segment, the previous refraction studies in B4 and B5 segments may give us some indications of the lithosphere structure and composition of the area. *Tolstoy et al.* [1995] showed that the crust within Segment B5 of the AAD is quite thin at ~4.2 km. Their model indicates that an unusually thin (~1.2 km) layer 3 underlies a layer 2 of normal thickness. A more recent refraction experiment in Segment B4 [*Kojima et al.*, 2003] yielded an anomalous velocity model, where P wave velocity gradually increases with depth to 7.8 km/s at a depth of only 3.6 km. Their study indicated that there is no layering structure beneath B4, and may support the idea that a compositionally heterogeneous lithosphere is formed when extension is dominated by detachment faulting [*Cannat*, 1993]. The amplitude of magnetic anomalies in the AAD is significantly weaker than in the surrounding areas [*Vogt et al.*, 1983; *Weissel and Hayes*, 1971]. This difference was attributed to the differences in Fe and Ti content between Zone A lavas and those of and Zones B and C [*Anderson et al.*, 1980], but the discovery of megamullion terrains suggests that the difference is more likely attributable to the anomalous lithospheric structure.

[31] The geometry and mechanism of the detachment fault plane is an important factor in understanding how oceanic lithosphere is developed under magma-starved conditions. Competing models with implications for the geometry and the characteristics on the fault plane at depth include: rooting of the detachment in the brittle-ductile transition at the base of the lithosphere [*Lavier et al.*, 1999; *Tucholke et al.*, 1998]; and rooting of the detachment in the shallower lithosphere where the serpentinization front may correspond to a rheological boundary and play a key role for fault initiation [*Escartín et al.*, 2003; *MacLeod et al.*, 2002]. The former hypothesis requires a steeply dipping fault plane with large rotations during fault movement, while the latter requires a shallow dipping fault plane with potentially much less exposure of deep sections of the oceanic lithosphere. The difference between these models can potentially be resolved by gravity and magnetic data. Although our data set is not adequate to resolve these models, a cross-axis profile across the largest B3E megamullion (Figure 7b) is consistent with a low-angle, shallow rooted detachment model. This profile shows low magnetization and high MBA on the north, hanging wall side of the axis ($-48.85°S \sim -49°S$), consistent with the presence of unaltered peridotite (high density and very low magnetization) at shallow depth.

5.2. Asymmetric Spreading

[32] The recent spreading history of subsegment B3E is dominated by extension on a detachment fault, leading to a remarkable degree of spreading asymmetry and the formation of a 50–55 km long megamullion terrain in less than 1 million years. In the same 1 million year period, only 10 km of new ocean crust has been added to the northern flank, and the full spreading rate has remained close to the 70 mm/yr rate predicted by the global plate model. Extreme asymmetric spreading is not confined to the inside corner of B3E, however. In Figures 9b and 9c, we show that unusually high half-spreading rates, with asymmetry up to 75%, coincide with some of the northern B3E megamullion terrains in addition to those of southern B3E. Asymmetric spreading also led to a change in the sense of the offset (from left to right/right to left) between B3E and B3W, as described in section 5.1 and Figure 10.

[33] Intervals during which detachment tectonics appear to have dominated the spreading process can also be inferred from existing data for other AAD segments (Figure 11). For Segments B4 and B5, we have calculated spreading rates and asymmetry factors using magnetic anomaly identifica-

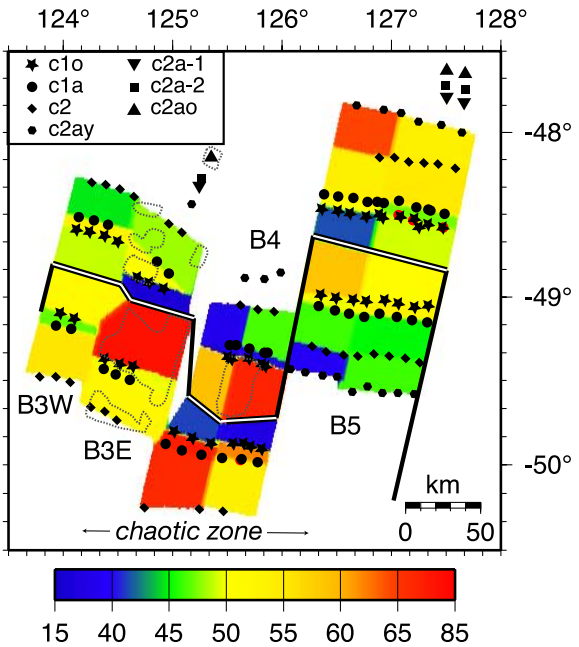

Figure 11. Crustal accretion rates for Segments B3, B4 and B5. Magnetic anomaly picks are shown as black symbols. The anomaly picks in B4 and B5 were provided by D. Wilson (personal communication, 2001) and were based on data collected during previous cruises. Double lines mark the ridge axes.

tions by D. Wilson (personal communication, 2001, based on magnetic profiles collected during previous cruises). Highly asymmetric spreading occurs in B3E, as reported here, across B4, and far off-axis (prior to c2) in B5 west. In B4 and B5 (as in B3) high spreading asymmetry corresponds to areas of chaotic seafloor morphology [*Christie et al.*, 1998].

[34] In an idealized model, asymmetry should be nearly 100% during intervals when extension is dominated by detachment faulting. Existing studies outside the AAD show, however, that this is rarely the case. For oceanic detachments along the Mid-Atlantic Ridge, spreading asymmetry is generally small or absent. This appears to be partly due to poor horizontal resolution associated with slow spreading rates and partly due to magmatic crustal accretion on the hanging wall. *Fujiwara et al.* [2003] identified the magnetic anomalies and showed that there are significant spreading asymmetries in two segments near the Fifteen-Twenty fracture zone. The asymmetry is, however, not so large and the horizontal resolution is not enough to correlate the area of apparent fast spreading with corrugated surfaces. *Allerton et al.* [2000] reported a case of extremely asymmetric crustal accretion accompanying a single, large fault near 29°N on the MAR. They concluded that magmatic accretion in this area has been effectively one sided, with new crust being added only to the outside corner, causing asymmetric spreading with polarity opposite to that of the AAD. This observation, combined with the common occurrence of gabbroic rocks on MAR detachment surfaces, suggests that melt production rates may remain high (relatively to spreading rate) on the MAR, even during episodes of detachment faulting.

[35] In the AAD, on the other hand, melt supply rates are uniformly low, reflecting the anomalously cold upper mantle beneath the region. Seismic layer 3 is very thin beneath the chaotic terrain of segment B5 [*Tolstoy et al.*, 1995] and seems not to exist at all beneath B4 [*Kojima et al.*, 2003]. Together with magnetic studies, these seismic observations confirm that melt production during extensional intervals in the AAD is anomalously low, especially relative to the faster spreading rate. This low melt supply, in turn, ensures the dominant role of detachment faulting in the spreading process. Although our off-axis data are limited to 40 miles off-axis, corresponding to approximately 2 Ma crust, asymmetric spreading has been recognized throughout the history of the AAD [*Cochran*, 1986; *Vogt et al.*, 1983; *Weissel and Hayes*, 1974]. A recent global compilation of asymmetric seafloor spreading [*Müller et al.*, 1998] shows that the southern flank of the AAD has spread faster, on average, at least since 10 Ma. This long-term asymmetry must be attributed primarily to ridge migration required by the absolute plate motions. It may, however, be accomplished by the accumulation of episodic, short-term asymmetries that are accommodated by oceanic detachment faults.

[36] Well developed oceanic detachments are now known to have formed at intermediate spreading rates in at least three places in addition to the AAD: the southernmost Central Indian Ridge (full spreading rate ~50 mm/yr) [*Mitchell et al.*, 1998]; the Chile Ridge (full spreading rate ~70 mm/yr) [*Martinez et al.*, 1998]; and at an extinct back arc spreading center in the Philippine Sea (estimated full spreading rate ~70 mm/yr) [*Ohara et al.*, 2001]. The large size of the Philippine Sea and AAD megamullions suggests a tendency toward larger megamullions at higher spreading rates, although no detailed analysis has yet been done. We speculate that the formation period of major

megamullion terrains may be relatively constant (~1–2 million years) at all intermediate to slow spreading rates, implying that the mode of spreading is not simply a function of spreading rate, but of the balance between melt supply and plate separation rate.

5.3. Extent of Chaotic Terrain

[37] *Christie et al.* [1998] pointed out that chaotic seafloor terrain within the AAD is a strong indicator of the dominance of tectonic extension over magmatic accretion at the spreading axis. A key observation of this study is that the chaotic terrain, and therefore the locus of asymmetric spreading and thin crust production is presently limited to Segments B3E and B4. Only 100 km of the axis appears to have produced anomalous oceanic lithosphere at least since 2 Ma. There is some uncertainty to this observation as there has been no off-axis mapping to the west of our survey area. However, a single multibeam swath along an E-W track near 48°S appears to record normal abyssal hill terrain with no indication of chaotic seafloor topography.

[38] The eastern boundary of the chaotic terrain was shown by *Christie et al.* [1998] to have migrated westward across Segment B5 between 4 Ma and present, although this migration appears to reflect a transient phenomenon [*Christie et al.*, 1998, 2004]. The terrain boundary in B5 corresponds to a geochemical boundary between Indian- and Pacific MORB mantle isotopic domains that is currently located at or near the B4/B5 segment boundary. Leg 187 of the Ocean Drilling Program [*Christie et al.*, 2004] traced this isotopic boundary from 14–28 Ma and showed that, since 28 Ma, it has remained within the eastern half of the depth anomaly. In contrast, the western boundary of the chaotic terrain has no known geochemical or isotopic expression, and it appears to have maintained a stable position relative to the axis for at least 2 Ma.

[39] The chaotic terrain does appear to correspond to the region of lowest melt production. *Klein et al.* [1991] showed from axial basalt geochemistry that the melt production rate is lowest in Segments B3 and B4. Crustal thickness estimates from geochemical data are also very low beneath this region [*Lecroart et al.*, 1997]. The anomalous shortage of melt supply may also be related to an anomalous thermal structure. Recent surface wave tomography near the AAD [*Ritzwoller et al.*, 2003] delineated a northwest-southeast trending low velocity anomaly that extends across the ocean basin, through the AAD. This anomaly is confined to the upper 120 km of the mantle and dips shallowly to the west. They estimated the crustal thinning averaged over the AAD to be about 4.8 km on the basis of an average temperature depression of 80°C in the upper 175 km. Because of the westward dip, the temperature depression should be larger and the melt deficit more prominent beneath B3E and B4 but definitive resolution is lacking at this fine scale. On a broader scale, *Gurnis et al.* [1998] proposed that the anomalously cool mantle temperatures beneath the AAD are derived from a stagnated subducted slab in the mantle transition zone. This slab originated at the long-lived Gondwanaland-Pacific convergent margin, and has been overridden by the rapidly migrating Australian plate since the Cretaceous. In their models, a fraction of the stagnant slab is entrained by upwelling mantle, creating a narrow, cold band beneath the eastern AAD. This simulation is, however, based on an unrealistic, uniform viscosity structure and its significance for realistic mantle conditions has not been demonstrated.

[40] Regardless of the validity or resolution of any given model, the abrupt change of morphological character at the chaotic terrain boundaries cannot be explained solely by regional mantle temperature anomalies. The large horizontal thermal gradients required are unlikely to be sustainable against the negative buoyancy of cold mantle [*Lin et al.*, 2002; *West et al.*, 1997]. The additional, and so far unknown, dynamic and/or petrological factors that must be involved require more detailed data and models for their solution.

6. Conclusion

[41] New bathymetry, magnetic and gravity data mainly from Segment B3 of the Australian-Antarctic Discordance (AAD) provide a wealth of new information on the distribution, mechanisms and origin of detachment faulting and its role as a dominant mechanism of seafloor spreading. Key observations and conclusions include the following:

[42] 1. Segment B3 is divided into two long-lived second-order segments of markedly contrasting character. The flanks of the western subsegment B3W are characterized by normal well-ordered abyssal hills. The flanks of B3E, on the other hand, are characterized by rough, chaotic terrain including several megamullions. The largest megamul-

lion terrain, at the inside corner of B3E, has 50–55 km long, continuous corrugations and is more than twice as large as typical megamullions of the MAR. Similar, but smaller domed structures with flow line parallel striations are distributed on both northern and southern flanks.

[43] 2. The megamullions in B3E are generally accompanied by 5∼10 mGal residual mantle Bouguer anomaly highs, indicating thinner crust and/or denser lithosphere. In contrast, a lower MBA anomaly values along B3W suggest that the crust is more normal along this subsegment.

[44] 3. High magnetization areas occur along the off-axis traces of nontransform discontinuities (NTD) and over the megamullion terrains of the southern flank of B3E most likely reflecting induced magnetization caused by peridotite serpentinization.

[45] 4. The association of chaotic seafloor morphology, thinner crust, megamullion structures and positive magnetization and high gravity indicate that extension along oceanic detachment faults has dominated the extension process in B3E and B4 for at least 2 million years. The presence of small megamullion terrains on the nondominant (north) flank indicates either that the polarity of detachment has reversed for short periods, or that periodic southward relocation of the detachment plane has isolated small sections of footwall and transferred them to the opposite (hanging wall) plate.

[46] 5. Since 2 Ma, the full-spreading rate has remained close to the 70 mm/yr rate predicted by the global plate motion model. Despite the rapid northward motion of the plate boundary, spreading in B3W is almost symmetrical. In contrast, B3E (and B4) is dominated by highly (and unusually) asymmetrical spreading, with asymmetries up to 75% over the largest megamullion terrains. These extreme asymmetries reflect an unusual imbalance between low magma supply and (relatively) rapid spreading rate.

[47] 6. The formation of chaotic seafloor terrain, reflecting a dominance of detachment faulting at the spreading axis, is presently restricted to a 100-km section of the axis in B3E and B4, apparently coinciding with the most magma-starved portion of the generally magma deficient AAD.

Acknowledgments

[48] We are grateful to the officers and crew of R/V *Hakuho-Maru* for their experienced support in data acquisition in very bad weather conditions. We thank the KH01-3 Leg 3 shipboard scientific party, M. Terazaki, M. Shinohara, K. Mochizuki, T. Yamada, K. Nakahigashi, and C. Igarashi for collaboration and discussion on board. We are also indebted to K. Tamaki for his support in planning and post-cruise studies. We deeply thank L. Géli and D. Wilson for allowing us to use their unpublished bathymetry and magnetic data in the surrounding areas, D. Blackman and an anonymous referee for their helpful reviews, and M. Coffin for his comments on an early draft of the paper. T. Fujiwara kindly helped us in analyzing the gravity data. The GMT software [*Wessel and Smith*, 1995] and MB system [*Caress and Chayes*, 1996] were extensively used in this study. Basic data processing and analysis of this work were mainly done by K. Matsuda as his master course study in the University of Tokyo. The study was supported by Japan Society for the Promotion of Science, Grant-in Aid for Scientific Researches (A)(2)11304024. Christie's participation was supported in part by the U.S. National Science Foundation.

References

Allerton, S., J. Escartín, and R. C. Searle (2000), Extremely asymmetric magmatic accretion of oceanic crust at the ends of slow-spreading ridge segments, *Geology*, *28*(2), 179–182.

Anderson, R. N., D. J. Spariosu, J. K. Weissel, and D. E. Hayes (1980), The interrelation between variations in magnetic anomaly amplitudes and basalt magnetization and chemistry along the Southeast Indian Ridge, *J. Geophys. Res.*, *85*(NB7), 3883–3898.

Blackman, D. K., J. R. Cann, B. Janssen, and D. K. Smith (1998), Origin of extensional core complexes: Evidence from the Mid-Atlantic Ridge at Atlantis Fracture Zone, *J. Geophys. Res.*, *103*(B9), 21,315–21,333.

Cande, S. C., and D. V. Kent (1995), Revised calibration of the geomagnetic polarity timescale for the Late Cretaceous and Cenozoic, *J. Geophys. Res.*, *100*(B4), 6093–6095.

Cande, S. C., and J. C. Mutter (1982), A revised identification of the oldest sea-floor spreading anomalies between Australia and Antarctica, *Earth Planet. Sci. Lett.*, *58*(2), 151–160.

Cann, J. R., D. K. Blackman, D. K. Smith, E. McAllister, B. Janssen, S. Mello, E. Avgerinos, A. R. Pascoe, and J. Escartín (1997), Corrugated slip surfaces formed at ridge-transform intersections on the Mid-Atlantic Ridge, *Nature*, *385*(6614), 329–332.

Cannat, M. (1993), Emplacement of mantle rocks in the seafloor at midocean ridges, *J. Geophys. Res.*, *98*(B3), 4163–4172.

Cannat, M., C. Rommevaux-Jestin, and H. Fujimoto (2003), Melt supply variations to a magma-poor ultra-slow spreading ridge (Southwest Indian Ridge 61° to 69°E), *Geochem. Geophys. Geosyst.*, *4*(8), 9104, doi:10.1029/2002GC000480.

Caress, D. W., and D. N. Chayes (1996), Improved processing of Hydrosweep DS multibeam data on the R/V Maurice Ewing, *Mar. Geophys. Res.*, *18*(6), 631–650.

Christie, D. M., B. P. West, D. G. Pyle, and B. B. Hanan (1998), Chaotic topography, mantle flow and mantle migration in the Australian-Antarctic discordance, *Nature*, *394*(6694), 637–644.

Christie, D. M., D. G. Pyle, R. B. Pedersen, and D. J. Miller (2004), Leg 187 Synthesis: History of the Australian Antarctic Discordance and the Indian-Pacific mantle isotopic boundary, *Proceedings of the Ocean Drilling Program,*

Scientific Results, vol. 187, edited by R. B. Pedersen, D. M. Christie, and D. J. Miller, Ocean Drill, Program, College Station, Tex. (Available at http://www-odp.tamu.edu/publications/187_SR/187sr.htm)

Cochran, J. R. (1986), Variations in subsidence rates along intermediate and fast spreading midocean ridges, *Geophys. J. R. Astron. Soc.*, *87*(2), 421–454.

Cochran, J. R., and M. Talwani (1977), Free-air gravity anomalies in world oceans and their relationship to residual elevation, *Geophys. J. R. Astron. Soc.*, *50*(3), 495–552.

Cochran, J. R., J. C. Sempéré, and S. S. Team (1997), The southeast Indian ridge between 88°E and 118°E: Gravity anomalies and crustal accretion at intermediate spreading rates, *J. Geophys. Res.*, *102*(B7), 15,463–15,487.

Davis, G. A., and G. S. Lister (1988), Detachment faulting in continental extension: Perspectives from the southwestern U.S. cordillera, *Spec. Pap. Geol. Soc. Am.*, *218*, 133–159.

Demets, C., R. G. Gordon, D. F. Argus, and S. Stein (1994), Effect of recent revisions to the geomagnetic reversal timescale on estimates of current plate motions, *Geophys. Res. Lett.*, *21*(20), 2191–2194.

Dick, H. J. B., et al. (2000), A long in situ section of the lower ocean crust: Results of ODP Leg 176 drilling at the Southwest Indian Ridge, *Earth Planet. Sci. Lett.*, *179*(1), 31–51.

Escartín, J., C. Mével, C. J. MacLeod, and A. M. McCaig (2003), Constraints on deformation conditions and the origin of oceanic detachments: The Mid-Atlantic Ridge core complex at 15°45′N, *Geochem. Geophys. Geosyst.*, *4*(8), 1067, doi:10.1029/2002GC000472.

Fujiwara, T., J. Lin, T. Matsumoto, P. B. Kelemen, B. E. Tucholke, and J. F. Casey (2003), Crustal Evolution of the Mid-Atlantic Ridge near the Fifteen-Twenty Fracture Zone in the last 5 Ma, *Geochem. Geophys. Geosyst.*, *4*(3), 1024, doi:10.1029/2002GC000364.

Gripp, A. E., and R. G. Gordon (1990), Current plate velocities relative to the hotspots incorporating the Nuvel-1 global plate motion model, *Geophys. Res. Lett.*, *17*(8), 1109–1112.

Gurnis, M., R. D. Müller, and L. Moresi (1998), Cretaceous vertical motion of Australia and the Australian- Antarctic discordance, *Science*, *279*(5356), 1499–1504.

Hayes, D. E. (1976), Nature and implications of asymmetric sea-floor spreading: Different rates for different plates, *Geol. Soc. Am. Bull.*, *87*(7), 994–1002.

Hayes, D. E. (1988), Age-depth relationships and depth anomalies in the southeast Indian Ocean and south Atlantic Ocean, *J. Geophys. Res.*, *93*(B4), 2937–2954.

Hayes, D. E., and J. R. Conolly (1972), Morphology of he southeast Indian Ocean, in *Antarctic Oceanology II: The Australian-New Zealand Sector*, *Antarctic Res. Ser.*, vol. 19, edited by D. E. Hayes, pp. 125–145, AGU, Washington, D. C.

Klein, E. M., C. H. Langmuir, A. Zindler, H. Staudigel, and B. Hamelin (1988), Isotope evidence of a mantle convection boundary at the Australian-Antarctic Discordance, *Nature*, *333*(6174), 623–629.

Klein, E. M., C. H. Langmuir, and H. Staudigel (1991), Geochemistry of basalts from the Southeast Indian Ridge, 115°E–138°E, *J. Geophys. Res.*, *96*(B2), 2089–2107.

Kojima, Y., M. Shinohara, K. Mochizuki, T. Yamada, K. Nakahigashi, and T. Kanazawa (2003), Seismic velocity structure in the Australian-Antarctic Discordance, Segment B4 revealed by airgun-OBS experiment, *Eos Trans. AGU*, *84*(46), Fall Meet. Suppl., Abstract S21F-0396.

Kuo, B. Y. (1993), Thermal anomalies beneath the Australian Antarctic Discordance, *Earth Planet. Sci. Lett.*, *119*(3), 349–364.

Kuo, B. Y., and D. W. Forsyth (1988), Gravity anomalies of the ridge-transform system in the south Atlantic between 31°S and 34.5°S: Upwelling centers and variations in crustal thickness, *Mar. Geophys. Res.*, *10*(3–4), 205–232.

Kuo, B. Y., S. H. Hung, and L. Y. Chiao (1995), A 3-D dynamic model for the anomalous topography and geoid over the South-East Indian Ridge, *Geophys. J. Int.*, *121*(1), 1–20.

Kuo, B. Y., C. H. Chen, and Y. S. Zhang (1996), A fast velocity anomaly to the west of the Australian-Antarctic discordance, *Geophys. Res. Lett.*, *23*(17), 2239–2242.

Lagabrielle, Y., D. Bideau, M. Cannat, J. A. Karson, and C. Mével (1998), Ultramafic-mafic plutonic rock suites exposed along the Mid-Atlantic Ridge (10°N–30°N): Symmetrical-asymmetrical distribution and implications for seafloor spreading processes, in *Faulting and Magmatism at Mid-Ocean Ridges*, *Geophys. Monogr. Ser.*, vol. 106, edited by W. R. Buck et al., pp. 153–176, AGU, Washington, D. C.

Lanyon, R., A. J. Crawford, and S. M. Eggins (1995), Westward migration of Pacific Ocean upper mantle into the Southern Ocean region between Australia and Antarctica, *Geology*, *23*(6), 511–514.

Lavier, L. L., W. R. Buck, and A. N. B. Poliakov (1999), Self-consistent rolling-hinge model for the evolution of large-offset low-angle normal faults, *Geology*, *27*(12), 1127–1130.

Lecroart, P., A. Cazenave, Y. Ricard, C. Thoraval, and D. G. Pyle (1997), Along-axis dynamic topography constrained by major-element chemistry, *Earth Planet. Sci. Lett.*, *149*(1–4), 49–56.

Lin, J., and J. Phipps Morgan (1992), The spreading rate dependence of 3-dimensional midocean ridge gravity structure, *Geophys. Res. Lett.*, *19*(1), 13–16.

Lin, S. C., L. Y. Chiao, and B. Y. Kuo (2002), Dynamic interaction of cold anomalies with the mid-ocean ridge flow field and its implications for the Australian-Antarctic Discordance, *Earth Planet. Sci. Lett.*, *203*(3–4), 925–935.

Macdonald, K. C., S. P. Miller, S. P. Huestis, and F. N. Spiess (1980), Three-dimensional modeling of a magnetic reversal boundary from inversion of deep-tow measurements, *J. Geophys. Res.*, *85*(NB7), 3670–3680.

Macdonald, K. C., P. J. Fox, R. T. Alexander, R. Pockalny, and P. Gente (1996), Volcanic growth faults and the origin of Pacific abyssal hills, *Nature*, *380*(6570), 125–129.

MacLeod, C. J., et al. (2002), Direct geological evidence for oceanic detachment faulting: The Mid-Atlantic Ridge, 15°45′N, *Geology*, *30*(10), 879–882.

Mandea, M., S. Macmillan, S. Bondar, V. Golovkov, B. Langlais, F. Lowes, N. Olsen, J. Quinn, and T. Sabaka (2000), International Geomagnetic Reference Field 2000, *Phys. Earth Planet. Inter.*, *120*, 39–42.

Marks, K. M., and J. M. Stock (1994), Variations in ridge morphology and depth-age relationships on the Pacific-Antarctic Ridge, *J. Geophys. Res.*, *99*(B1), 531–541.

Marks, K. M., P. R. Vogt, and S. A. Hall (1990), Residual depth anomalies and the origin of the Australian- Antarctic Discordance zone, *J. Geophys. Res.*, *95*(B11), 17,325–17,337.

Marks, K. M., D. T. Sandwell, P. R. Vogt, and S. A. Hall (1991), Mantle downwelling beneath the Australian-Antarctic Discordance zone—Evidence from geoid height versus topography, *Earth Planet. Sci. Lett.*, *103*(1–4), 325–338.

Martinez, F., J. Karsten, and E. M. Klein (1998), Recent kinematics and tectonics of the Chile Ridge, *Eos Trans. AGU*, *79*(45), Fall Meet. Suppl., F836.

Mitchell, N. C., J. Escartín, and S. Allerton (1998), Detachment faults at mid-ocean ridges garner interest, *Eos Trans. AGU*, *79*, 127.

Müller, R. D., W. R. Roest, and J. Y. Royer (1998), Asymmetric sea-floor spreading caused by ridge-plume interactions, *Nature*, *396*(6710), 455–459.

Mutter, J. C., K. A. Hegarty, S. C. Cande, and J. K. Weissel (1985), Breakup between Australia and Antarctica: A brief review in the light of new data, *Tectonophysics*, *114*(1–4), 255–279.

Ohara, Y., T. Yoshida, Y. Kato, and S. Kasuga (2001), Giant megamullion in the Parece Vela Backarc Basin, *Mar. Geophys. Res.*, *22*(1), 47–61.

Palmer, J. E. B., J. C. Sempéré, D. M. Christie, and J. Phipps Morgan (1993), Morphology and tectonics of the Australian-Antarctic Discordance between 123°E and 128°E, *Mar. Geophys. Res.*, *15*(2), 121–152.

Pariso, J. E., C. Rommevaux, and J. C. Sempéré (1996), Three-dimensional inversion of marine magnetic anomalies: Implications for crustal accretion along the Mid-Atlantic Ridge (28°–31°30′N), *Mar. Geophys. Res.*, *18*(1), 85–101.

Parker, R. L. (1972), Rapid calculation of potential anomalies, *Geophys. J. R. Astron. Soc.*, *31*(4), 447–455.

Parker, R. L., and S. P. Huestis (1974), Inversion of magnetic anomalies in the presence of topography, *J. Geophys. Res.*, *79*(11), 1587–1593.

Phipps Morgan, J., and D. W. Forsyth (1988), Three-dimensional flow and temperature perturbations due to a transform offset: Effects on oceanic crustal and upper mantle structure, *J. Geophys. Res.*, *93*(B4), 2955–2966.

Pockalny, R. A., A. Smith, and P. Gente (1995), Spatial and temporal variability of crustal magnetization of a slowly spreading ridge: Mid-Atlantic Ridge (20°–24°N), *Mar. Geophys. Res.*, *17*(3), 301–320.

Prince, R. A., and D. W. Forsyth (1988), Horizontal extent of anomalously thin crust near the Vema Fracture Zone from the three-dimensional analysis of gravity anomalies, *J. Geophys. Res.*, *93*(B7), 8051–8063.

Pyle, D. G., D. M. Christie, and J. J. Mahoney (1992), Resolving an isotopic boundary within the Australian Antarctic Discordance, *Earth Planet. Sci. Lett.*, *112*(1–4), 161–178.

Ranero, C. R., and T. J. Reston (1999), Detachment faulting at ocean core complexes, *Geology*, *27*(11), 983–986.

Ritzwoller, M. H., N. M. Shapiro, and G. M. Leahy (2003), A resolved mantle anomaly as the cause of the Australian-Antarctic Discordance, *J. Geophys. Res.*, *108*(B12), 2559, doi:10.1029/2003JB002522.

Sandwell, D. T., and W. H. F. Smith (1997), Marine gravity anomaly from Geosat and ERS 1 satellite altimetry, *J. Geophys. Res.*, *102*(B5), 10,039–10,054.

Searle, R. C., M. Cannat, K. Fujioka, C. Mével, H. Fujimoto, A. Bralee, and L. Parson (2003), FUJI Dome: A large detachment fault near 64°E on the very slow-spreading southwest Indian Ridge, *Geochem. Geophys. Geosyst.*, *4*(8), 9105, doi:10.1029/2003GC000519.

Tivey, M. A., and B. E. Tucholke (1998), Magnetization of 0–29 Ma ocean crust on the Mid-Atlantic Ridge, 25°30′ to 27°10′N, *J. Geophys. Res.*, *103*(B8), 17,807–17,826.

Tolstoy, M., A. J. Harding, J. A. Orcutt, and J. Phipps Morgan (1995), Crustal thickness at the Australian-Antarctic discordance and neighboring Southeast Indian Ridge, *Eos Trans. AGU*, *76*(46), Fall Meet. Suppl., F570.

Tucholke, B. E., and J. Lin (1994), A geological model for the structure of ridge segments in slow- spreading ocean crust, *J. Geophys. Res.*, *99*(B6), 11,937–11,958.

Tucholke, B. E., J. Lin, and M. C. Kleinrock (1998), Megamullions and mullion structure defining oceanic metamorphic core complexes on the Mid-Atlantic Ridge, *J. Geophys. Res.*, *103*(B5), 9857–9866.

Veevers, J. J. (1982), Australian Antarctic depression from the mid-ocean ridge to adjacent continents, *Nature*, *295*(5847), 315–317.

Vogt, P. R., N. Z. Cherkis, and G. A. Morgan (1983), Project Investigator-I: Evolution of the Australia-Antarctic discordance deduced from a detailed aeromagnetic study, in *Antarctic Earth Science: 4th International Symposium*, edited by R. L. Oliver, P. R. James, and J. B. Jago, pp. 608–613, Aust. Acad. of Sci., Camberra, A. C. T., Australia.

Weissel, J. K., and D. E. Hayes (1971), Asymmetric seafloor spreading south of Australia, *Nature*, *231*(5304), 518–522.

Weissel, J. K., and D. E. Hayes (1974), Australian-Antarctic Discordance: New results and implications, *J. Geophys. Res.*, *79*(17), 2579–2587.

Wessel, P., and W. H. F. Smith (1995), New version of Generic Mapping Tools released, *Eos Trans. AGU*, *76*, 329.

West, B. P., J. C. Sempéré, D. G. Pyle, J. Phipps Morgan, and D. M. Christie (1994), Evidence for variable upper-mantle temperature and crustal thickness in and near the Australian Antarctic Discordance, *Earth Planet. Sci. Lett.*, *128*(3–4), 135–153.

West, B. P., W. S. D. Wilcock, J. C. Sempéré, and L. Geli (1997), Three-dimensional structure of asthenospheric flow beneath the Southeast Indian Ridge, *J. Geophys. Res.*, *102*(B4), 7783–7802.